THE JOURNAL OF PHYSICAL CHEMISTRY C

Article

pubs.acs.org/JPCC

Efficiency of Interfacial Electron Transfer from Zn-Porphyrin Dyes into TiO_2 Correlated to the Linker Single Molecule Conductance

Christian F. A. Negre,[†,‡] Rebecca L. Milot,[†] Lauren A. Martini,[†] Wendu Ding,[†] Robert H. Crabtree,*[,†,‡] Charles A. Schmuttenmaer,[†,‡,*] and Victor S. Batista*[,†,‡]

[†]Department of Chemistry, Yale University, 225 Prospect St., P.O. Box 208107, New Haven, Connecticut, 06520-8107 United States

[‡]Energy Sciences Institute, Yale University, P.O. Box 27394, West Haven, Connecticut, 06516-7394 United States

Supporting Information

ABSTRACT: High performance dye-sensitized solar cells (DSSCs) rely upon molecular linkers that allow efficient electron transport from the photoexcited dye into the conduction band of the semiconductor host substrate. We have studied photoinduced electron injection efficiencies from modular assemblies of a Zn-porphyrin dye and a series of linker molecules which are axially bound to the Zn-porphyrin complex and covalently bound to TiO_2 nanoparticles. Experimental measurements based on terahertz spectroscopy are compared to the calculated molecular conductance of the linker molecules. We find a linear relationship between measured electron injection efficiency and calculated single-molecule conductance of the linker employed. Since the same chromophore is used in all cases, variations in the absorptivities of the adsorbate complexes are quite small and cannot account for the large variations in observed injection efficiencies. These results suggest that the linker single-molecule conductance is a key factor that should be optimized for maximum electron injection efficiencies in DSSCs. In addition, our findings demonstrate for the first time the possibility of inferring values of single molecule conductance for bridging molecules at semiconductor interfaces by using time-resolved THz spectroscopy.

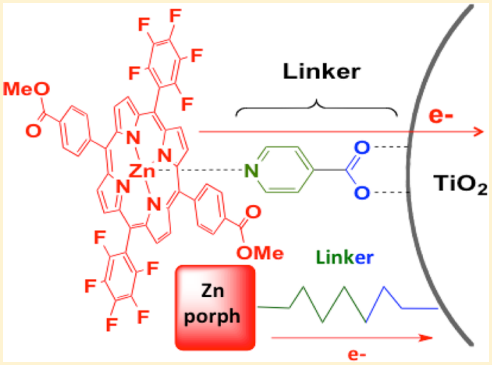

1. INTRODUCTION

Ever since the seminal work of O'Regan and Grätzel,[1] dye-sensitized solar cells (DSSCs) have continued to raise significant interest as promising alternatives for solar-to-electric energy conversion. DSSCs are particularly attractive since they are based on inexpensive semiconductor materials (typically nanoporous TiO_2, ZnO, or SnO_2)[2−5] sensitized to visible light absorption with dyes covalently attached to the semiconductor surface by molecular linkers. Photoexcitation of the sensitizer dye leads to electron−hole pair separation, injecting electrons through the molecular linkers into the conduction band (CB) of the semiconductor surface. The photogenerated electron carriers then flow through the external load toward the cathode, performing useful electrical work along the way. At the cathode, electrons reduce a redox mediator (e.g., I_3^-), generating a redox species (e.g., I^-) which refills the holes left behind on the sensitizer molecules.[2,6] While significant research effort has been devoted to the study of DSSCs, the outstanding challenge is to improve the photoconversion efficiency. Here, we focus on the transport properties of the molecular linkers as directly correlated to the efficiency of electron injection into the semiconductor.

A variety of dyes for DSSCs have been explored beyond the initially utilized Ru−polypyridyl complexes, including inexpensive alternatives such as π-conjugated organic molecules that bypass the need of precious metals.[7−11] These organic dyes are promising because they exhibit large $\pi-\pi^*$ excitation cross sections and absorb strongly in the visible region of the spectrum.[12−18] Organic DSSCs with efficiencies up to 11% have been prepared very recently.[19] Zn-porphyrin dyes, which have been incorporated in some of the most efficient DSSCs to date,[20,21] are particularly attractive since they have high molar absorptivity. In addition, the spectral and electronic properties can be tuned by varying both the centrally coordinated metal ion and the peripheral substituents.[22−24] Metal porphyrins can bind directly to the semiconductor surface via built-in anchoring groups at the beta- and meso-positions or alternatively through linkers that coordinate to the metal center in the axial position (Figure 1a).[25−28] The advantage of the axial binding motif is that it separates the design and synthesis of the linker from the development of the porphyrin dye, thereby simplifying the design of the chromophore/redox active center and assembly of the molecular framework to the semiconductor surface. Nevertheless, axial linkers have been much less investigated, compared to anchoring groups substituting at the beta or meso positions of the porphyrin ring. It is therefore important to analyze the efficiency of photoinduced electron injection as a function of the linker structure[25] and explore structure/function relations that might

Received: August 31, 2013
Revised: October 21, 2013
Published: October 23, 2013

   dx.doi.org/10.1021/jp408738b | J. Phys. Chem. C 2013, 117, 24462−24470

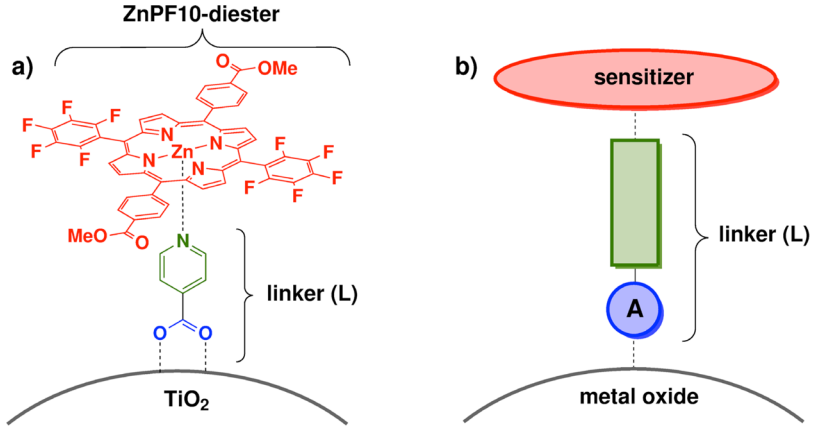

Figure 1. (a) $ZnPF_{10}$-diester bound to TiO_2 via a pyridyl linker using the modular assembly technique. (b) Cartoon depiction of the modular assembly method for attaching Zn porphyrins to TiO_2 via simple molecular linkers with varying anchor groups. The porphyrin sensitizer, linker (L), and anchors (A) are described in the text.

correlate the resulting interfacial electron transfer efficiency with the electrical properties of the linkers.

High-potential porphryin dyes have been assembled in photoanodes for DSSCs[29] as well as in photocatalytic cells for light-driven water splitting when codeposited with a water oxidation catalyst on TiO_2 thin films.[30] They were found to be quite versatile since they could be optimized to give sufficiently positive redox potentials, as necessary to activate catalysts for water oxidation. Furthermore, when covalently bound to semiconductor surfaces, they were stable under oxidative and aqueous conditions, as necessary for photocatalytic water oxidation. However, the reported cells have shown low efficiency calling for fundamental studies of the factors responsible for efficiency loss.

In addition to the optimization of the spectral and electrochemical properties of the dye, optimum performance requires assemblies that maximize electron injection into the semiconductor.[31−35] For metal-porphyrins bound through axial coordination, electron injection can be optimized through suitable design and refinement of the molecular linker.[36] Two photoinjection mechanisms are possible: photoexcitation of the dye, followed by injection through the molecular linker (type-I), or direct injection from the ground state of the dye to the CB of the semiconductor (type-II).[37−40] While both mechanisms involve ultrafast time scales,[41,42] the type-I process is usually favored in porphyrin dyes as well as in the molecular assemblies most commonly used in DSSCs.[43] Therefore, it is important to focus on optimization of interfacial electron injection by design of molecular linkers that provide proper alignment of electronic states and strong electronic coupling with the semiconductor CB.

Several experimental techniques have been used to study photoinjection mechanisms in DSSCs and to determine the efficiency and time scales of interfacial electron transfer at a variety of semiconductor surfaces, including transient absorption spectroscopy, electron paramagnetic resonance, and time-resolved terahertz (THz) spectroscopy.[5,44−50] In addition, analytical studies and computational simulations of interfacial electron transfer have advanced our understanding of the complex interrelation between the dye and the semiconductor surface.[23,40,51−59] These studies have shown that highly conductive linkers, such as molecular frameworks with conjugated double bonds, usually inject carriers much faster than aliphatic linkers. In addition, several studies have focused on the differences in electron injection observed for different anchoring groups.[25,60−63] However, a systematic study of the molecular origin of differences in the efficiency of interfacial electron injection has yet to be reported. In this work, we employ a series of modular linker-porphyrin assemblies that vary in their anchoring group for surface attachment. We find that the efficiency of interfacial electron injection as probed by THz spectroscopy correlates with the single molecule conductance of the linkers binding Zn-porphyrin dyes to TiO_2 surfaces. The resulting insight is particulary relevant to the design of linker-porphyrin assemblies when combined with optimization of photoabsorption and redox properties by inverse design techniques.[36] These findings also demonstrate for the first time the possibility of inferring values of single molecule conductance by using time-resolved THz spectroscopy for molecules bridging electron donor adsorbates at semiconductor interfaces.

2. EXPERIMENTAL AND COMPUTATIONAL METHODS

2.1. Sample Preparation. All compounds were obtained or synthesized from commercially available starting materials and were used without further purification unless otherwise noted. Isonicotinic acid (L1) and 4-pyridyl-boronic acid (L5) were obtained from Aldrich. The molecular linkers 4-pyridyl-phosphonic acid (L2), 4-pyridyl-acetylacetonate (L3), and 4-pyridyl-hydroxamic acid (L5) were synthesized according to a previously reported literature procedure.[64−68] The high-potential zinc porphyrin dye $ZnPF_{10}$-diester was also synthesized according to a previously reported literature procedure.[29,30]

Mesoporous thin films of TiO_2 were prepared using Degussa Aeroxide P25 titanium dioxide nanoparticles by either doctor-blading or spin-coating. Films used for absorbance measurements were prepared on microscope coverslips (25 × 25 mm for spin-coating, 22 × 50 mm for doctor-blading, Fisherbrand, USA). Films used for time-resolved THz spectroscopy measurements were prepared on fused quartz microscope slides (1 × 1 in, 1 mm thickness, GM Associates, Inc., USA). Bare TiO_2 thin films were soaked overnight in the dark in a 0.5 mM solution of the desired linker (L1-L5) in ethanol and thoroughly rinsed with ethanol to remove unbound linker. The films were dried at room temperature for at least 30 min, soaked overnight in the dark in a 0.1 mM dichloromethane solution of the $ZnPF_{10}$-diester porphyrin, and rinsed well with

dx.doi.org/10.1021/jp408738b | J. Phys. Chem. C 2013, 117, 24462−24470

dichloromethane to remove any uncoordinated or aggregated porphyrin.

Absorption spectra were recorded using a Cary 3E UV−visible spectrophotometer (Agilent Technologies). Thin films of TiO_2 were highly scattering so absorbance spectra of all thin films were taken in diffuse reflectance geometry using an integrating sphere attachment.

2.2. Time-Resolved THz Spectroscopy (TRTS) Measurements. An amplified Ti:sapphire laser (Tsunami/Spitfire from Spectra Physics) generated 800 mW of pulsed near-IR light at a 1 kHz repetition rate. The pulse width was ∼130 fs, and the center wavelength was 800 nm. Roughly two-thirds of the power was frequency doubled and then filtered to produce 40 mW of 400 nm (3.1 eV) light for the pump beam. The remainder of the near-IR light was used to generate THz radiation via optical rectification in a ZnTe(110) crystal and detect it using free space electro optic sampling in a second ZnTe(110) crystal. Terahertz data were taken at room temperature, and the average of two samples was taken for each data set. Further information on the spectrometer and technique can be found in the literature.[45,69−71]

2.3. Conductance and Electronic Structure Calculations. The steady state current flowing through the molecular linker has been computed according to the Landauer−Büttiker formula[72,73]

$$I = \frac{2e}{h}\int_{\mu_L}^{\mu_R} T(E)\,\mathrm{d}E \tag{1}$$

where e is the electron charge, h is Planck's constant, μ_L and μ_R are the chemical potentials for the electron in the left and right leads, respectively (Figure 2), and E is the energy of the conducting channel. The transmission function T is calculated by using the Fisher−Lee formula[74]

$$T = Tr(g^{+}_{dev}(E)\Gamma_L(E)g^{-}_{dev}(E)\Gamma_R(E)) \tag{2}$$

where $g^{+}_{dev}(E)$ is the advanced nonequilibrium Green's function (NEGF) operator for the system consisting of the device attached to one-dimensional leads, as shown in Figure 2.[75]

The NEGF operator can be written, as follows:

$$g_{dev}(z) = (zS - H_{dev} - \Sigma_L(z) - \Sigma_R(z))^{-1} \tag{3}$$

where z is the generalized complex energy variable, S is the overlap matrix, H_{dev} is the Hamiltonian of the molecule, and Σ_L and Σ_R are the self-energy operators corresponding to the left and right leads, respectively. Γ is defined as follows:

$$\Gamma_{L/R} = i(\Sigma^{+}_{L/R}(E) - \Sigma^{-}_{L/R}(E)) \tag{4}$$

where $\Sigma^{+}_{L/R}(E)$ and $\Sigma^{-}_{L/R}(E)$ are the advanced and retarded self-energy operators for the left (L) and right (R) contacts, respectively.

The electronic structure and transport properties of the linkers were determined by using the semiempirical extended-Hückel (EH) Hamiltonian in conjunction with the NEGF methodology.[76−78] In the basis of localized atomic orbitals, the matrices $\Sigma_{L/R}$ are assumed to be diagonal with nonzero elements $(\Sigma_{L/R})_{11} = \gamma^2 g_0^{+L}(E)$ and $(\Sigma_{L/R})_{NN} = \gamma^2 g_0^{+R}(E)$ where the indices $1 - N$ label the atomic orbitals of the linker that have significant overlap with the left and right leads. The parameter γ defines the effective electronic coupling with the contacts and is assumed to the same for s, p, and d orbitals. The Green's function for the isolated left and right contacts, $g_0^{+L/R} = -i/|\beta|$, are defined to mimic semi-infinite one-dimensional nanowires as described by a nearest-neighbor tight-binding Hamiltonian with constant intersite coupling β.[79] The value of $\gamma^2/|\beta| = 2.0$ eV was chosen to ensure that the conductance of a linear chain of gold atoms at 0 V bias is equal to the unit of quantum conductance (i.e., $G_0 = 2e^2/h$) when connected to the model nanowire leads, as recently reported.[78] All calculations of conductance were performed at 0 V bias. Hence

$$G = \frac{2e^2}{h}T(E_F) \tag{5}$$

where G is the molecular conductance (in Siemens), and the transmission function T is evaluated at the device Fermi level E_F. The geometries of the linkers (Figure 3) correspond to optimized minimum energy configurations, obtained via density functional theory (DFT) at the B3LYP/LANL2DZ level, as implemented in Gaussian 09.[80]

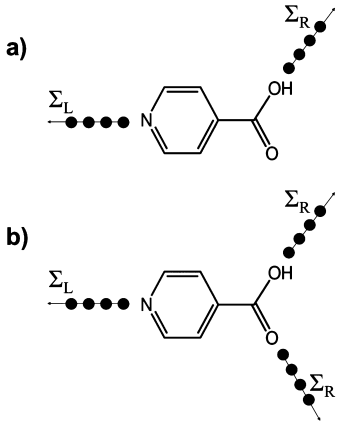

Figure 2. Scheme depicting the coupling of 4-pyridyl-carboxylic acid to the semi-infinite leads in monodentate (a) and bidentate (b) binding motifs.

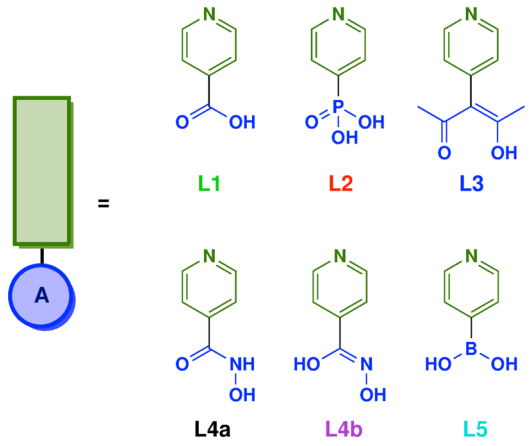

Figure 3. Linker molecules (L) substituted with different anchoring groups (A) that covalently bind Zn-porphyrin sensitizers to TiO_2 surfaces. Linkers have the structure 4-pyridyl-A, where the anchoring group A is either carboxylic acid (L1), phosphonic acid (L2), acetylacetonate (L3) hydroxamic acid (L4), or boronic acid (L5).

dx.doi.org/10.1021/jp408738b | J. Phys. Chem. C 2013, 117, 24462−24470

3. RESULTS AND DISCUSSION

Figure 3 shows the structures of the linkers analyzed in this study. All the linkers have the form 4-pyridyl-A where the anchoring group A is either carboxylic acid (L1), phosphonic acid (L2), acetylacetonate (L3), hydroxamic acid (L4), or boronic acid (L5). Hydroxamic acid is treated in both of its two tautomers L4a and L4b.[81] These anchoring groups are known to bind strongly to semiconductor surfaces while the pyridyl group axially coordinates to the metal center of the prophyrin $ZnPF_{10}$ through the pyridyl nitrogen, sensitizing the TiO_2 surface (Figure 1).[82] These surface-bound complexes are collectively denoted L-$ZnPF_{10}$, with L = L1−L5.

Figure 4 shows the UV−vis diffuse reflectance spectra of the L-$ZnPF_{10}$ assemblies bound to TiO_2 showing only small differences in the molar absorptivity of the chromophore-linker assemblies. In fact, Figure 4 shows that L1-$ZnPF_{10}$, L2-$ZnPF_{10}$, and L4-$ZnPF_{10}$ have nearly the same absorbance at around 400 nm, which is the wavelength of the pump pulse in our THz measurements, while the absorptivities of L3-$ZnPF_{10}$ (shown) and L5-$ZnPF_{10}$ (not shown) are only slightly lower. Therefore, differences in the observed photoinjection yields of these assemblies cannot be attributed to differences in light-harvesting efficiency.

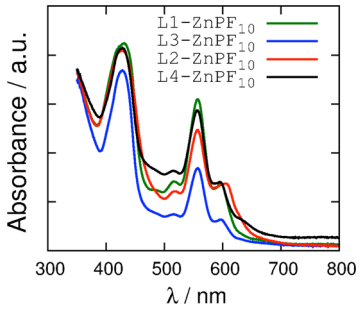

Figure 4. Experimental UV−vis diffuse reflectance spectra for L-$ZnPF_{10}$ complexes covalently bound to nanoporous TiO_2 thin films.

Figure 5 shows the change in transmitted THz amplitude as a function of time after the TiO_2 thin-films sensitized with L-$ZnPF_{10}$ are photoexcited with a pump pulse at 400 nm. The attenuation of THz amplitude is a measure of the efficiency of electron injection, since it is proportional to the concentration of free charge carriers injected into the semiconductor conduction band (denoted state *B* in Figure 6).[45,71,83,84] As a control experiment, we note there is no detectable attenuation of THz transmittance when $ZnPF_{10}$ is merely physisorbed on the TiO_2 surface, whereas all of the L-$ZnPF_{10}$ complexes covalently bound to the surface show measurable attenuation. We also performed a seccond control experiment that shows no injection from porphyrin-free L1-sensitized anatase compared to the full system (L1-$ZnPF_{10}$; see Figure S4). Since the predominant porphyrin excitation near 400 nm (the Soret or B band) arises from the $S_2 \leftarrow S_0$ transition, which is $\pi^* \leftarrow \pi$, these results suggest that the photoinjected carriers must travel through the linkers (or through space) in order to be injected into TiO_2. From the THz data alone, however, we see significant differences in the efficiency of electron injection for the different anchoring groups. The efficiencies of electron injection for the various L-$ZnPF_{10}$ complexes can be ranked according to the order: L4 > L1 > L2 ≈ L3 ≈ L5.

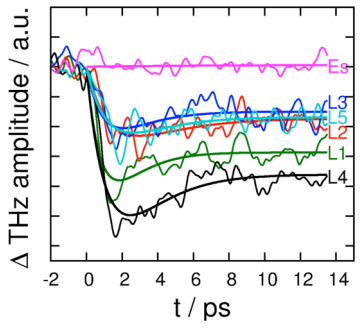

Figure 5. Change in THz amplitude (thin lines) measured as a function of time after photoexcitation at 400 nm for L-$ZnPF_{10}$ assemblies covalently bound to TiO_2 surfaces as shown in Figure 1. Thick lines are best fitting curves determined by the kinetic model described in the text (eq 6). As a control, the magenta corresponds to $ZnPF_{10}$-diester (Es) physisorbed to the TiO_2 surface in the absence of a molecular linker.

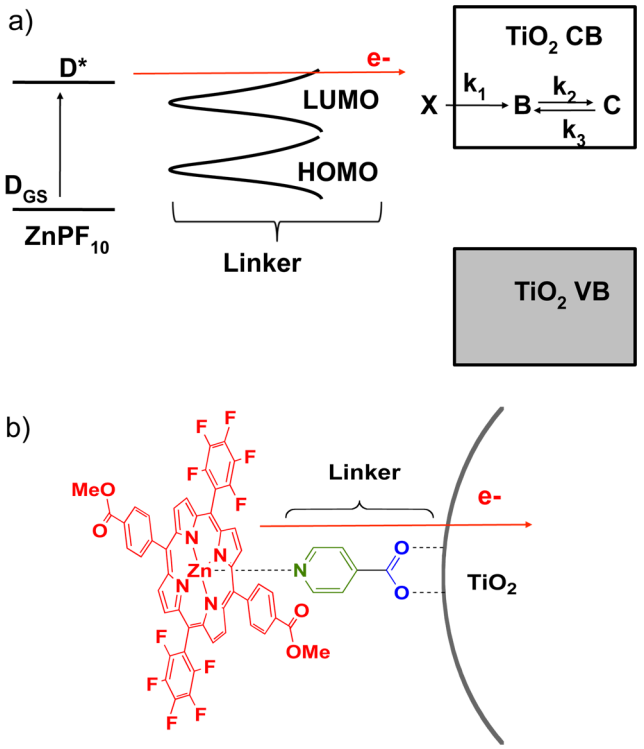

Figure 6. Schematic diagram of photoinjection in terms of the most relevant energy levels (a) and molecular structures (b). D_{GS} and D* correspond to the porphyrin dye $ZnPF_{10}$ in the ground (S_0) and second excited state (S_2), respectively. *X* represents the carrier concentration at the TiO_2 surface prior to injection, *B* is the concentration of free carriers injected into the TiO_2 conduction band, and *C* is the concentration of trapped carriers.

Figure 6 shows a schematic diagram of the photoinjection process. Upon photoexcitation of the dye, electrons are transferred through the pyridyl ligand and anchoring group to the semiconductor surface (D* → X). This is an ultrafast[51] electron transmission process that takes a few femtoseconds prior to the interfacial injection of free carriers into the conduction band (X → B with an injection rate constant k_1 of tens to hundreds of femtoseconds). The kinetic model also includes trapping (B → C) and detrapping (C → B) dynamics with rate constants k_2 and k_3, respectively. According to this

dx.doi.org/10.1021/jp408738b | J. Phys. Chem. C 2013, 117, 24462−24470

kinetic model, the concentration of free carriers B, as a function of time t, is given by the following equation:

$$B(t) = X_0(\theta_1 + \theta_2 e^{-k_1 t} + \theta_3 e^{-(k_2+k_3)t}) \quad (6)$$

where

$$\theta_1 = \frac{k_3}{k_2 + k_3}$$

$$\theta_2 = \frac{(k_1 - k_3)}{-k_1 + k_2 + k_3}$$

$$\theta_3 = \frac{k_1 k_2}{(k_2 + k_3)(k_1 - k_2 - k_3)} \quad (7)$$

The derivation of eqs 6 and 7 is provided in the Supporting Information (SI). Equation 6 provides a description of the time-dependent concentration of free carriers that should be proportional to the observed attenuation of THz transmitted amplitude for the different anchoring groups. The trapping and detrapping rate constants k_2 and k_3 are assumed to depend only on the nature of the semiconductor and therefore are treated as global fitting parameters common to all anchoring groups. The parameter X_0, which is reported in Table 1 for each linker, gives

Table 1. Calculated Conductance Values (G) for Linkers in Monodentate and Bidentate Binding Modes and the Maximum Change in THz Amplitude X_0[a]

	conductance, $G/10^3$ nS		
linker	bidentate	monodentate	X_0/arb. units
L1	(2.11)	7.26	6.95
L2	(7.90)	3.99	4.56
L3	2.37	(1.16)	3.76
L4-a	13.36	(3.50)	9.31
L4-b	6.27	(2.99)	9.31
L5	(5.77)	2.76	4.29

[a]Bracketed values do not correlate with X_0 since they do not correspond to the proper binding mode of the ligand (bidentate for L3 and L4 and monodentate for L1, L2 and L5).

a measure of the efficiency of photoinjection as probed by THz spectroscopy since it is proportional to the THz amplitude at the time of maximum attentuation, t_m, and therefore proportional to the concentration of electrons injected into the semiconductor conduction band.

For comparison, Table 1 also reports the values of single molecule conductance computed for each linker by using the EH NEGF methodology outlined in section 2.3. Values for L3 and L4 were calculated assuming a bidentate binding mode, while L1, L2, and L5 were assumed to have monodentate binding. The attachment mode (bidentate for L3 and L4 and monodentate for L1, L2, and L5) is determined for each ligand according to the DFT minimum energy configuration (Figure S5, SI). Our results are consistent with the special arrangement of oxygen atoms, separated by more than two bonds in L3 and L4 anchoring groups, leading to a configuration that is more favorable for bidentate binding with Ti^{4+} octahedral sites.[49,50] Monodentate binding is found to be most stable for L1, L2, and L5, consistent with previous reports for L1,[85] L2,[61] and L5.[86,87] Also, crystallographic data for the dyes absorbed onto novel $(TiO_2)_{17}$ clusters shows a bidentate chelating mode for L3.[88]

The case of L4 has been previouselly modeled showing a favorable bidentate oxygen vacancy mode.[50]

The conductance value for L4 was taken as the average between the conductance values for L4a and L4b[81] because the DFT computed energy diference between the two conformers is less than 0.1 eV.

Figure 7 shows the correlation of the maximum change in THz amplitude X_0 as a function of the linker conductance in

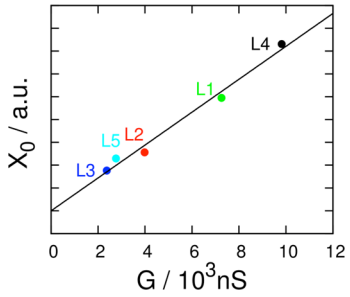

Figure 7. Change in THz amplitude (X_0) at the time of maximum attenuation (t_m) versus conductance G computed for the various linkers. The best linear fit is given by $X_0 = 0.7212G + 1.9943$, with $R^2 = 0.9851$.

the L-$ZnPF_{10}$ complexes. The linear relationship ($R^2 = 0.9851$), suggests that the transport properties of the different linkers have a direct effect on the electron injection and efficiency. The observed correlation between electron injection efficiency and calculated molecular conductance provides a valuable guideline for designing new sensitizers. To understand why different linkers have different values of conductances, we analyze the electronic structure/function relations for the different linkers as correlated to their transport properties.

Figure 8 displays the frontier molecular orbitals of linkers L1 and L3 that are primarily responsible for electron transport.

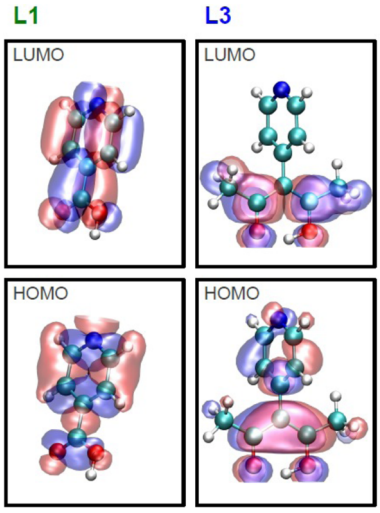

Figure 8. Frontier orbitals calculated within the EH level of theory for L1 and L3.

(Analogous frontier orbitals for L2, L4, and L5 are provided in the SI, Figure S2.) Although L1 and L3 are both known to bind well to the TiO_2 surface,[2,49] L1 has higher conductance and yields much more efficient electron injection than L3. Figure 8 shows that these differences can be attributed to differences in the electronic structure since the pyridine ring of L3 is rotated

dx.doi.org/10.1021/jp408738b | J. Phys. Chem. C 2013, 117, 24462−24470

nearly perpendicularly to the anchoring group and therefore is not conjugated with the electronic structure of the anchor as in L1. Furthermore, the LUMO orbital of L3 is localized on the anchor and therefore does not provide good electronic coupling with the pyridine moiety. In contrast, the LUMO of L1 is delocalized along the entire linker, providing an efficient channel for electron transport.

The analysis of L2 and L5 suggests that phosphonic acid (L2) and boronic acid (L5) functional groups decrease the overall conductance since those functional groups inhibit electron tunneling when bound to the semiconductor surface. In contrast, the hydroxamate linker L4 binds as a bidentate ligand, leading to a more efficient injection than through the monodentate L1 linker.[57] When compared to the bidentate L3 ligand, L4 also leads to much more efficient electron injection due to the extended conjugation and delocalization of the LUMO over the entire linker. EH Frontier orbitals for all the ligands are ploted in Figure S2 in the SI.

The D* → X transport is the primary electron transfer event in porphyrin type-I modular assemblies following photoabsorption at 400 nm due to $\pi^* \leftarrow \pi$ photoexcitation. The photoabsorption and D* → X transport events, however, are dynamically decoupled since the transition dipole moment of the Soret band lies in the plane of the porphyrin ring,[89] which is parallel to the TiO_2 surface. The resulting decoupling with respect to the adiabatic photoinjection[90] is consistent with the observation that the photoabsorption features remain almost unchanged when using linkers with different electron transport efficiency. Figure 9 shows the projected DOS (pDOS) for two

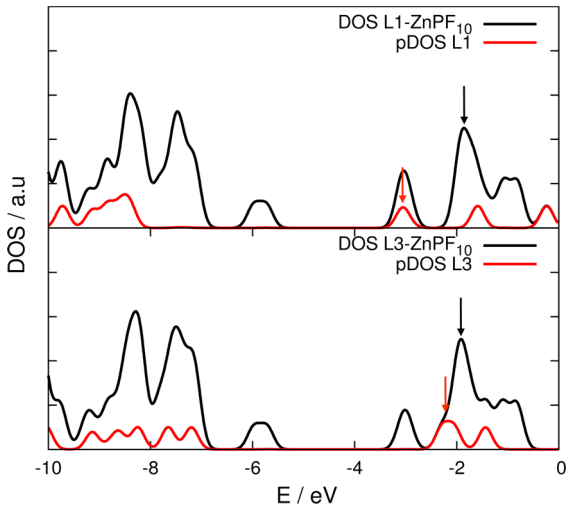

Figure 9. Total density of states (DOS) of the L1-$ZnPF_{10}$ and L3-$ZnPF_{10}$ assemblies (black) and projected DOS onto the linkers L1 and L3 (red). The Fermi level is around −4.44 eV. Red arrows indicating the LUMO for the linker projection. Black arrows indicating the final orbitals participating in the D* → D transition.

of the L-$ZnPF_{10}$ complexes, revealing that the LUMO of the pyridine ligand (red arrows) should be the main orbital responsible for transmission of electrons from the $ZnPF_{10}$ to the conduction band of TiO_2 as it is located right under the porphirin projected excited state (black arrows). DOS for all L-$ZnPF_{10}$ are also shown in Figure S3. These findings suggest that the axial modular assembling technique should be particularly useful for isolating the effect of electron transport properties during electron photoinjection from the photoabsorption properties of the porphyrin dye.

4. CONCLUSIONS

We have studied the efficiency of interfacial electron injection from Zn-porphyrin dyes bound to TiO_2 surfaces via axially coordinated pyridine ligands with a variety of different anchoring groups. The photoconversion efficiency has been characterized by the attenuation of transmitted time-resolved terahertz (THz) signal after photoexcitation and interfacial electron transfer. We found a linear relationship between the interfacial electron injection efficiency and the single molecule conductance of the linker computed according to the nonequilibrium Green's function formalism. This simple relationship suggests that pyridyl linkers in the surface-bound L-$ZnPF_{10}$ complexes function as effective molecular wires, transmitting photoexcited electrons from the light-absorbing porphyrin sensitizer into the conduction band of TiO_2. These results are particularly relevant for optimization of DSSCs that rely upon molecular linkers mediating electron transport from the dye into the conduction band of the semiconductor host substrate. In addition, these findings demonstrate for the first time the possibility of inferring values of single molecule conductance by using time-resolved THz spectroscopy to probe bridging molecules that covalently bind dyes to semiconductor surfaces, while keeping constant the other components of the molecular assembly, such as the nature of the dye and the semiconductor material.

■ ASSOCIATED CONTENT

Ⓢ Supporting Information

Kinetic model and derivation of eq 6; additional figures with the analysis of relaxed configurations, THz analysis; density of states, frontier orbitals, and absorption spectra; coordinates for optimized structures; sample input file for geometry optimizations in SIESTA; and full Gaussian 09 reference. This material is available free of charge via the Internet at http://pubs.acs.org.

■ AUTHOR INFORMATION

Corresponding Authors

*E-mail: robert.crabtree@yale.edu.
*E-mail: charles.schmuttenmaer@yale.edu.
*E-mail: victor.batista@yale.edu.

Notes

The authors declare no competing financial interest.

■ ACKNOWLEDGMENTS

We acknowledge support by the U.S. Department of Energy Grant DE-FG02-07ER15909 (C.A.S) and DE-PS02-08ER15944 (R.H.C). Computational work was supported as part of the Argonne-Northwestern Solar Energy Research (ANSER) Center, an Energy Frontier Research Center funded by the U.S. Department of Energy, Office of Science, Office of Basic Energy Sciences under Award Number DE-SC0001059 (V.S.B). Computer resources were provided by NERSC and by the High performance Computing facilities at Yale University.

■ REFERENCES

(1) O'Regan, B.; Grätzel, M. A Low-Cost, High-Efficiency Solar-Cell Based on Dye-Sensitized Colloidal Tio_2 Films. *Nature* **1991**, *353*, 737−740.

(2) Hagfeldt, A.; Boschloo, G.; Sun, L. C.; Kloo, L.; Pettersson, H. Dye-Sensitized Solar Cells. *Chem. Rev.* **2010**, *110*, 6595−6663.
(3) Beek, W. J. E.; Wienk, M. M.; Janssen, R. A. J. Hybrid Solar Cells from Regioregular Polythiophene and ZnO Nanoparticles. *Adv. Funct. Mater.* **2006**, *16*, 1112−1116.
(4) Kwong, C. Y.; Choy, W. C. H.; Djurisic, A. B.; Chui, P. C.; Cheng, K. W.; Chan, W. K. Poly(3-hexylthiophene): TiO_2 Nanocomposites for Solar Cell Applications. *Nanotechnology* **2004**, *15*, 1156−1161.
(5) Yoshihara, T.; Katoh, R.; Furube, A.; Murai, M.; Tamaki, Y.; Hara, K.; Murata, S.; Arakawa, H.; Tachiya, M. Quantitative Estimation of the Efficiency of Electron Injection from Excited Sensitizer Dye Into Nanocrystalline ZnO Film. *J. Phys. Chem. B* **2004**, *108*, 2643−2647.
(6) Privalov, T.; Boschloo, G.; Hagfeldt, A.; Svensson, P. H.; Kloo, L. A Study of the Interactions between I-/I-3(-) Redox Mediators and Organometallic Sensitizing Dyes in Solar Cells. *J. Phys. Chem. C* **2009**, *113*, 783−790.
(7) Bessho, T.; Yoneda, E.; Yum, J. H.; Guglielmi, M.; Tavernelli, I.; Imai, H.; Rothlisberger, U.; Nazeeruddin, M. K.; Grätzel, M. New Paradigm in Molecular Engineering of Sensitizers for Solar Cell Applications. *J. Am. Chem. Soc.* **2009**, *131*, 5930−5934.
(8) Grätzel, M. Solar Energy Conversion by Dye-Sensitized Photovoltaic Cells. *Inorg. Chem.* **2005**, *44*, 6841−6851.
(9) Grätzel, M. Recent Advances in Sensitized Mesoscopic Solar Cells. *Acc. Chem. Res.* **2009**, *42*, 1788−1798.
(10) Grätzel, M. Photoelectrochemical Cells. *Nature* **2001**, *414*, 338−344.
(11) Mishra, A.; Fischer, M. K. R.; Bauerle, P. Metal-Free Organic Dyes for Dye-Sensitized Solar Cells: From Structure: Property Relationships to Design Rules. *Angew. Chem.-Int. Edit.* **2009**, *48*, 2474−2499.
(12) Qin, P.; Zhu, H. J.; Edvinsson, T.; Boschloo, G.; Hagfeldt, A.; Sun, L. C. Design of an Organic Chromophore For P-Type Dye-Sensitized Solar Cells. *J. Am. Chem. Soc.* **2008**, *130*, 8570−8571.
(13) Chen, K. F.; Hsu, Y. C.; Wu, Q. Y.; Yeh, M. C. P.; Sun, S. S. Structurally Simple Dipolar Organic Dyes Featuring 1,3-Cyclohexadiene Conjugated Unit for Dye-Sensitized Solar Cells. *Org. Lett.* **2009**, *11*, 377−380.
(14) Horiuchi, T.; Miura, H.; Sumioka, K.; Uchida, S. High Efficiency of Dye-Sensitized Solar Cells Based on Metal-Free Indoline Dyes. *J. Am. Chem. Soc.* **2004**, *126*, 12218−12219.
(15) Chen, J. H.; Tsai, C. H.; Wang, S. A.; Lin, Y. Y.; Huang, T. W.; Chiu, S. F.; Wu, C. C.; Wong, K. T. Organic Dyes Containing a Coplanar Indacenodithiophene Bridge for High-Performance Dye-Sensitized Solar Cells. *J. Org. Chem.* **2011**, *76*, 8977−8985.
(16) Hoth, C. N.; Schilinsky, P.; Choulis, S. A.; Brabec, C. J. Printing Highly Efficient Organic Solar Cells. *Nano Lett.* **2008**, *8*, 2806−2813.
(17) Kuang, D.; Walter, P.; Nuesch, F.; Kim, S.; Ko, J.; Comte, P.; Zakeeruddin, S. M.; Nazeeruddin, M. K.; Grätzel, M. Co-Sensitization of Organic Dyes for Efficient Ionic Liquid Electrolyte-Based Dye-Sensitized Solar Cells. *Langmuir* **2007**, *23*, 10906−10909.
(18) Mei, J. G.; Graham, K. R.; Stalder, R.; Reynolds, J. R. Synthesis of Isoindigo-Based Oligothiophenes for Molecular Bulk Heterojunction Solar Cells. *Org. Lett.* **2010**, *12*, 660−663.
(19) Zhang, M.; Wang, Y.; Xu, M.; Ma, W.; Li, R.; Wang, P. Design of High-Efficiency Organic Dyes for Titania Solar Cells Based On The Chromophoric Core of Cyclopentadithiophene-Benzothiadiazole. *Energy Environ. Sci.* **2013**, *6*, 2944−2949.
(20) Yella, A.; Lee, H.-W.; Tsao, H. N.; Yi, C.; Chandiran, A. K.; Nazeeruddin, M. K.; Diau, E. W.-G.; Yeh, C.-Y.; Zakeeruddin, S. M.; Grätzel, M. Porphyrin-Sensitized Solar Cells with Cobalt (II/III)−Based Redox Electrolyte Exceed 12% Efficiency. *Science* **2011**, *334*, 629−634.
(21) Bessho, T.; Zakeeruddin, S. M.; Yeh, C.-Y.; Diau, E. W.-G.; Grätzel, M. Highly Efficient Mesoscopic Dye-Sensitized Solar Cells Based on Donor−Acceptor-Substituted Porphyrins. *Angew. Chem., Int. Ed.* **2010**, *49*, 6646−6649.
(22) Imahori, H.; Umeyama, T.; Ito, S. Large pi-Aromatic Molecules as Potential Sensitizers for Highly Efficient Dye-Sensitized Solar Cells. *Acc. Chem. Res.* **2009**, *42*, 1809−1818.
(23) Lin, C. Y.; Wang, Y. C.; Hsu, S. J.; Lo, C. F.; Diau, E. W. G. Preparation and Spectral, Electrochemical, and Photovoltaic Properties of Acene-Modified Zinc Porphyrins. *J. Phys. Chem. C* **2010**, *114*, 687−693.
(24) Campbell, W. M.; Burrell, A. K.; Officer, D. L.; Jolley, K. W. Porphyrins as Light Harvesters in The Dye-Sensitised Tio_2 Solar Cell. *Coord. Chem. Rev.* **2004**, *248*, 1363−1379.
(25) Martini, L. A.; Moore, G. F.; Milot, R. L.; Cai, L. Z.; Sheehan, S. W.; Schmuttenmaer, C. A.; Brudvig, G. W.; Crabtree, R. H. Modular Assembly of High-Potential Zinc Porphyrin Photosensitizers Attached to TiO_2 with a Series of Anchoring Groups. *J. Phys. Chem. C* **2013**, *117*, 14526−14533.
(26) Brumbach, M. T.; Boal, A. K.; Wheeler, D. R. Metalloporphyrin Assemblies on Pyridine-Functionalized Titanium Dioxide. *Langmuir* **2009**, *25*, 10685−10690.
(27) Subbaiyan, N. K.; Hill, J. P.; Ariga, K.; Fukuzumi, S.; D'Souza, F. Enhanced Photocurrents via Redox Modulation By Fluoride Binding to Oxoporphyrinogen in a Zinc Porphyrin-Oxoporphyrinogen Surface Modified TiO_2 Supramolecular Solar Cell. *Chem. Commun.* **2011**, *47*, 6003−6005.
(28) Subbaiyan, N. K.; Wijesinghe, C. A.; D'Souza, F. Supramolecular Solar Cells: Surface Modification of Nanocrytalline TiO_2 with Coordinating Ligands To Immobilize Sensitizers and Dyads via Metal-Ligand Coordination for Enhanced Photocurrent Generation. *J. Am. Chem. Soc.* **2009**, *131*, 14646−14647.
(29) Moore, G. F.; Konezny, S. J.; Song, H. E.; Milot, R. L.; Blakemore, J. D.; Lee, M. L.; Batista, V. S.; Schmuttenmaer, C. A.; Crabtree, R. H.; Brudvig, G. W. Bioinspired High-Potential Porphyrin Photoanodes. *J. Phys. Chem. C* **2012**, *116*, 4892−4902.
(30) Moore, G. F.; Blakemore, J. D.; Milot, R. L.; Hull, J. F.; Song, H. E.; Cai, L.; Schmuttenmaer, C. A.; Crabtree, R. H.; Brudvig, G. W. A Visible Light Water-Splitting Cell with a Photoanode Formed By Codeposition of a High-Potential Porphyrin and an Iridium Water-Oxidation Catalyst. *Energy Environ. Sci.* **2011**, *4*, 2389−2392.
(31) Stockwell, D.; Yang, Y.; Huang, J.; Anfuso, C.; Huang, Z. Q.; Lian, T. Q. Comparison of Electron-Transfer Dynamics from Coumarin 343 to TiO_2, SnO_2, and ZnO Nanocrystalline Thin Films: Role of Interface-Bound Charge-Separated Pairs. *J. Phys. Chem. C* **2010**, *114*, 6560−6566.
(32) Nazeeruddin, M. K.; De Angelis, F.; Fantacci, S.; Selloni, A.; Viscardi, G.; Liska, P.; Ito, S.; Bessho, T.; Grätzel, M. Combined Experimental and DFT-TDDFT Computational Study of Photoelectrochemical Cell Ruthenium Sensitizers. *J. Am. Chem. Soc.* **2005**, *127*, 16835−16847.
(33) Lin, L. Y.; Tsai, C. H.; Wong, K. T.; Huang, T. W.; Hsieh, L.; Liu, S. H.; Lin, H. W.; Wu, C. C.; Chou, S. H.; Chen, S. H.; et al. Organic Dyes Containing Coplanar Diphenyl-Substituted Dithienosilole Core for Efficient Dye-Sensitized Solar Cells. *J. Org. Chem.* **2010**, *75*, 4778−4785.
(34) Snaith, H. J.; Zakeeruddin, S. M.; Wang, Q.; Pechy, P.; Grätzel, M. Dye-Sensitized Solar Cells Incorporating a "Liquid" Hole-Transporting Material. *Nano Lett.* **2006**, *6*, 2000−2003.
(35) Pensack, R. D.; Asbury, J. B. Beyond the Adiabatic Limit: Charge Photogeneration in Organic Photovoltaic Materials. *J. Phys. Chem. Lett.* **2010**, *1*, 2255−2263.
(36) Xiao, D. Q.; Martini, L. A.; Snoeberger, R. C.; Crabtree, R. H.; Batista, V. S. Inverse Design and Synthesis of acac-Coumarin Anchors for Robust TiO_2 Sensitization. *J. Am. Chem. Soc.* **2011**, *133*, 9014−9022.
(37) De Angelis, F. Direct vs. Indirect Injection Mechanisms in Perylene Dye-Sensitized Solar Cells: A DFT/TDDFT Investigation. *Chem. Phys. Lett.* **2010**, *493*, 323−327.
(38) Tae, E. L.; Lee, S. H.; Lee, J. K.; Yoo, S. S.; Kang, E. J.; Yoon, K. B. A Strategy to Increase the Efficiency of the Dye-Sensitized TiO_2 Solar Cells Operated By Photoexcitation of Dye-to-TiO_2 Charge-Transfer Bands. *J. Phys. Chem. B* **2005**, *109*, 22513−22522.

(39) Koops, S. E.; Barnes, P. R. F.; O'Regan, B. C.; Durrant, J. R. Kinetic Competition in a Coumarin Dye-Sensitized Solar Cell: Injection and Recombination Limitations upon Device Performance. *J. Phys. Chem. C* **2010**, *114*, 8054−8061.
(40) De Angelis, F.; Fantacci, S.; Selloni, A. Alignment Of The Dye's Molecular Levels With The Tio_2 Band Edges In Dye-Sensitized Solar Cells: a DFT-TDDFT Study. *Nanotechnology* **2008**, *19*, 424002.
(41) Duncan, W. R.; Stier, W. M.; Prezhdo, O. V. Ab Initio Nonadiabatic Molecular Dynamics of the Ultrafast Electron Injection Across The Alizarin-TiO_2 Interface. *J. Am. Chem. Soc.* **2005**, *127*, 7941−7951.
(42) Duncan, W. R.; Prezhdo, O. V. Theoretical Studies of Photoinduced Electron Transfer in Dye-Sensitized TiO_2. *Annu. Rev. Phys. Chem.* **2007**, *58*, 143−184.
(43) Oviedo, M. B.; Zarate, X.; Negre, C. F. A.; Schott, E.; Arratia-Perez, R.; Sanchez, C. G. Quantum Dynamical Simulations as a Tool for Predicting Photoinjection Mechanisms in Dye-Sensitized TiO_2 Solar Cells. *J. Phys. Chem. Lett.* **2012**, *3*, 2548−2555.
(44) Ramakrishna, G.; Ghosh, H. N.; Singh, A. K.; Palit, D. K.; Mittal, J. P. Dynamics of Back-Electron Transfer Processes of Strongly Coupled Triphenyl Methane Dyes Adsorbed On TiO_2 Nanoparticle Surface as Studied by Fast and Ultrafast Visible Spectroscopy. *J. Phys. Chem. B* **2001**, *105*, 12786−12796.
(45) Turner, G. M.; Beard, M. C.; Schmuttenmaer, C. A. Carrier Localization And Cooling in Dye-Sensitized Nanocrystalline Titanium Dioxide. *J. Phys. Chem. B* **2002**, *106*, 11716−11719.
(46) Wang, Y. H.; Hang, K.; Anderson, N. A.; Lian, T. Q. Comparison of Electron Transfer Dynamics in Molecule-to-Nanoparticle and Intramolecular Charge Transfer Complexes. *J. Phys. Chem. B* **2003**, *107*, 9434−9440.
(47) Anderson, N. A.; Lian, T. Q. Ultrafast Electron Transfer at the Molecule-Semiconductor Nanoparticle Interface. *Annu. Rev. Phys. Chem.* **2005**, *56*, 491−519.
(48) Furube, A.; Katoh, R.; Hara, K.; Sato, T.; Murata, S.; Arakawa, H.; Tachiya, M. Lithium Ion Effect on Electron Injection from a Photoexcited Coumarin Derivative into a TiO_2 Nanocrystalline Film Investigated by Visible-to-IR Ultrafast Spectroscopy. *J. Phys. Chem. B* **2005**, *109*, 16406−16414.
(49) McNamara, W. R.; Snoeberger, R. C.; Li, G.; Schleicher, J. M.; Cady, C. W.; Poyatos, M.; Schmuttenmaer, C. A.; Crabtree, R. H.; Brudvig, G. W.; Batista, V. S. Acetylacetonate Anchors for Robust Functionalization of TiO_2 Nanoparticles with Mn(II)-Terpyridine Complexes. *J. Am. Chem. Soc.* **2008**, *130*, 14329−14338.
(50) McNamara, W. R.; Snoeberger, R. C.; Li, G. H.; Richter, C.; Allen, L. J.; Milot, R. L.; Schmuttenmaer, C. A.; Crabtree, R. H.; Brudvig, G. W.; Batista, V. S. Hydroxamate Anchors for Water-Stable Attachment to TiO_2 Nanoparticles. *Energ. Environ. Sci.* **2009**, *2*, 1173−1175.
(51) Rego, L. G. C.; Batista, V. S. Quantum Dynamics Simulations of Interfacial Electron Transfer in Sensitized TiO_2 Semiconductors. *J. Am. Chem. Soc.* **2003**, *125*, 7989−7997.
(52) Duncan, W. R.; Prezhdo, O. V. Nonadiabatic Molecular Dynamics Study of Electron Transfer from Alizarin to the Hydrated Ti^{4+} ion. *J. Phys. Chem. B* **2005**, *109*, 17998−18002.
(53) Duncan, W. R.; Prezhdo, O. V. Temperature Independence Of the Photoinduced Electron Injection in Dye-Sensitized TiO_2 Rationalized by Ab Initio Time-Domain Density Functional Theory. *J. Am. Chem. Soc.* **2008**, *130*, 9756−9762.
(54) Sanchez-de-Armas, R.; Lopez, J. O.; San-Miguel, M. A.; Sanz, J. F.; Ordejon, P.; Pruneda, M. Real-Time TD-DFT Simulations in Dye Sensitized Solar Cells: The Electronic Absorption Spectrum of Alizarin Supported on TiO_2 Nanoclusters. *J. Chem. Theory Comput.* **2010**, *6*, 2856−2865.
(55) Li, J. R.; Kondov, I.; Wang, H. B.; Thoss, M. Theoretical Study of Photoinduced Electron-Transfer Processes in the Dye- Semiconductor System Alizarin-TiO_2. *J. Phys. Chem. C* **2010**, *114*, 18481−18493.
(56) Rocca, D.; Gebauer, R.; De Angelis, F.; Nazeeruddin, M. K.; Baroni, S. Time-Dependent Density Functional Theory Study Of Squaraine Dye-Sensitized Solar Cells. *Chem. Phys. Lett.* **2009**, *475*, 49−53.
(57) Jakubikova, E.; Snoeberger, R. C.; Batista, V. S.; Martin, R. L.; Batista, E. R. Interfacial Electron Transfer in TiO_2 Surfaces Sensitized with Ru(II)-Polypyridine Complexes. *J. Phys. Chem. A* **2009**, *113*, 12532−12540.
(58) Kusama, H.; Sugihara, H.; Sayama, K. Nitrogen-Containing Heterocycles' Interaction with Ru Dye in Dye-Sensitized Solar Cells. *J. Phys. Chem. C* **2009**, *113*, 20764−20771.
(59) Odom, S. A.; Kelley, R. F.; Ohira, S.; Ensley, T. R.; Huang, C.; Padilha, L. A.; Webster, S.; Coropceanu, V.; Barlow, S.; Hagan, D. J.; et al. Photophysical Properties of an Alkyne-Bridged Bis(zinc porphyrin)-Perylene Bis(dicarboximide) Derivative. *J. Phys. Chem. A* **2009**, *113*, 10826−10832.
(60) Ernstorfer, R.; Gundlach, L.; Felber, S.; Storck, W.; Eichberger, R.; Willig, F. Role of Molecular Anchor Groups In Molecule-To-Semiconductor Electron Transfer. *J. Phys. Chem. B* **2006**, *110*, 25383−25391.
(61) Nilsing, M.; Persson, P.; Ojamae, L. Anchor Group Influence on Molecule-Metal Oxide Interfaces: Periodic Hybrid DFT Study of Pyridine Bound to TiO_2 via Carboxylic and Phosphonic Acid. *Chem. Phys. Lett.* **2005**, *415*, 375−380.
(62) She, C. X.; Guo, J. C.; Irle, S.; Morokuma, K.; Mohler, D. L.; Zabri, H.; Odobel, F.; Youm, K. T.; Liu, F.; Hupp, J. T.; et al. Comparison of Interfacial Electron Transfer Through Carboxylate And Phosphonate Anchoring Groups. *J. Phys. Chem. A* **2007**, *111*, 6832−6842.
(63) McNamara, W. R.; Milot, R. L.; Song, H. E.; Snoeberger, R. C.; Batista, V. S.; Schmuttenmaer, C. A.; Brudvig, G. W.; Crabtree, R. H. Water-Stable, Hydroxamate Anchors for Functionalization of Tio_2 Surfaces with Ultrafast Interfacial Electron Transfer. *Energy Environ. Sci.* **2010**, *3*, 917−923.
(64) Hirao, T.; Masunaga, T.; Ohshiro, Y.; Agawa, T. A Novel Synthesis of Dialkyl Arenephosphonates. *Synth.-Stuttgart.* **1981**, *1*, 56−57.
(65) Konar, S.; Zoń, J.; Prosvirin, A. V.; Dunbar, K. R.; Clearfield, A. Synthesis and Characterization of Four Metal−Organophosphonates with One-, Two-, and Three-Dimensional Structures. *In. Chem.* **2007**, *46*, 5229−5236.
(66) Mackay, L. G.; Anderson, H. L.; Sanders, J. K. M. A Platinum-Linked Porphyrin Trimer and a Complementary Aluminium tris[3-(4-pyridyl)acetylacetonate] Guest. *J. Chem. Soc.-Perkin Trans.* **1995**, *1*, 2269−2273.
(67) Mulcahy, C.; Krot, K. A.; Griffith, D. M.; Suponitsky, K. Y.; Starikova, Z. A.; Marmion, C. J. Iron(III) Tris(pyridinehydroxamate)s and Related Nickel(II) and Zinc(II) Complexes: Potential Platforms for the Design of Novel Heterodimetallic Supramolecular Assemblies. *Eur. J. Inorg. Chem.* **2007**, *10*, 1373−1380.
(68) Spampinato, V.; Tuccitto, N.; Quici, S.; Calabrese, V.; Marletta, G.; Torrisi, A.; Licciardello, A. Functionalization of Oxide Surfaces by Terpyridine Phosphonate Ligands: Surface Reactions and Anchoring Geometry. *Langmuir* **2010**, *26*, 8400−8406.
(69) Beard, M. C.; Turner, G. M.; Schmuttenmaer, C. A. Transient Photoconductivity in GaAs as Measured by Time-Resolved Terahertz Spectroscopy. *Phys. Rev. B* **2000**, *62*, 15764−15777.
(70) Beard, M. C.; Turner, G. M.; Schmuttenmaer, C. A. Subpicosecond Carrier Dynamics in Low-Temperature Grown GaAs as Measured by Time-Resolved Terahertz Spectroscopy. *J. Appl. Phys.* **2001**, *90*, 5915−5923.
(71) Baxter, J. B.; Schmuttenmaer, C. A. Conductivity of ZnO Nanowires, Nanoparticles, and Thin Films Using Time-Resolved Terahertz Spectroscopy. *J. Phys. Chem. B* **2006**, *110*, 25229−25239.
(72) Landauer, R. Electrical Resistance of Disordered One-Dimensional Lattices. *Philos. Mag.* **1970**, *21*, 863−872.
(73) Buttiker, M. 4-Terminal Phase-Coherent Conductance. *Phys. Rev. Lett.* **1986**, *57*, 1761−1764.
(74) Fisher, D. S.; Lee, P. A. Relation Between Conductivity and Transmission Matrix. *Phys. Rev. B* **1981**, *23*, 6851−6854.

(75) Xue, Y. Q.; Datta, S.; Ratner, M. A. First-Principles Based Matrix Green's Function Approach To Molecular Electronic Devices: General Formalism. *Chem. Phys.* **2002**, *281*, 151−170.
(76) Andrews, D. Q.; Cohen, R.; Van Duyne, R. P.; Ratner, M. A. Single Molecule Electron Transport Junctions: Charging and Geometric Effects on Conductance. *J. Chem. Phys.* **2006**, *125*, 174718.
(77) Negre, C. F. A.; Jara, G. E.; Vera, D. M. A.; Pierini, A. B.; Sanchez, C. G. Detailed Analysis of Water Structure in a Solvent Mediated Electron Tunneling Mechanism. *J. Phys.: Condens. Matter* **2011**, *23*, 245305.
(78) Paz, S. A.; Zoloff, M. M. E.; Negre, C. F. A.; Olmos-Asar, J. A.; Mariscal, M. M.; Sánchez, C. G.; Leiva, E. P. M. Configurational Behavior and Conductance of Alkanedithiol Molecular Wires from Accelerated Dynamics Simulations. *J. Chem. Theory Comput.* **2012**, *8*, 4539−4545.
(79) Todorov, T. N.; Briggs, G. A. D.; Sutton, A. P. Elastic Quantum Transport Through Small Structures. *J. Phys.: Condens. Matter* **1993**, *5*, 2389−2406.
(80) Frisch, M. J.; et al. *Gaussian 09*, revision *A.1*; Gaussian, Inc.: Wallingford, CT, 2009.
(81) Yale, H. L. The Hydroxamic Acids. *Chem. Rev.* **1943**, *33*, 209−256.
(82) Morandeira, A.; López-Duarte, I.; Martínez-Díaz, M. V.; O'Regan, B.; Shuttle, C.; Haji-Zainulabidin, N. A.; Torres, T.; Palomares, E.; Durrant, J. R. Slow Electron Injection On Ru−Phthalocyanine Sensitized TiO_2. *J. Am. Chem. Soc.* **2007**, *129*, 9250−9251.
(83) Richter, C.; Schmuttenmaer, C. A. Exciton-Like Trap States Limit Electron Mobility in TiO_2 Nanotubes. *Nat. Nanotechnol.* **2010**, *5*, 769−772.
(84) Brauer, J. C.; Moser, J.-E. Transient Photoconductivity of Dye-Sensitized TiO_2 Nanocrystalline Films Probed by Optical Pump-THz Probe Spectroscopy. In *17th International Conference on Ultrafast Phenomena*; Chergui, M., Jonas, D. M., Riedle, E., Schoenlein, R. W., Taylor, A. J., Eds.; Oxford University Press: New York, 2011; pp 358−360.
(85) Vittadini, A.; Selloni, A.; Rotzinger, F. P.; Grätzel, M. Formic Acid Adsorption on Dry and Hydrated TiO_2 Anatase (101) Surfaces by DFT Calculations. *J. Phys. Chem. B* **2000**, *104*, 1300−1306.
(86) Ambrosio, F.; Martsinovich, N.; Troisi, A. What Is the Best Anchoring Group for a Dye in a Dye-Sensitized Solar Cell? *J. Phys. Chem. Lett.* **2012**, *3*, 1531−1535.
(87) Raghunath, P.; Lin, M. C. Adsorption Configurations and Reactions of Boric Acid on a TiO_2 Anatase (101) Surface. *J. Phys. Chem. C* **2008**, *112*, 8276−8287.
(88) Snoeberger, R. C.; Young, K. J.; Tang, J.; Allen, L. J.; Crabtree, R. H.; Brudvig, G. W.; Coppens, P.; Batista, V. S.; Benedict, J. B. Interfacial Electron Transfer into Functionalized Crystalline Polyoxotitanate Nanoclusters. *J. Am. Chem. Soc.* **2012**, *134*, 8911−8917.
(89) Oviedo, M. B.; Sanchez, C. G. Transition Dipole Moments of the Q(y) Band in Photosynthetic Pigments. *J. Phys. Chem. A* **2011**, *115*, 12280−12285.
(90) Koyama, Y.; Kakitani, Y.; Nagae, H. Mechanisms of Suppression and Enhancement of Photocurrent/Conversion Efficiency in Dye-Sensitized Solar-Cells Using Carotenoid and Chlorophyll Derivatives as Sensitizers. *Molecules* **2012**, *17*, 2188−2218.

■ NOTE ADDED AFTER ASAP PUBLICATION

This paper was published ASAP on November 8, 2013, with an error to the affiliations and reference errors to Sections 2 and 3. The corrected version was reposted November 11, 2013.